Naval Research Laboratory
Washington, DC 20375-5320

NRL/MR/6790--08-9163

Laser-Pumped Coherent X-Ray FEL

PHILLIP SPRANGLE
JOSEPH PEÑANO

Beam Physics Branch
Plasma Physics Division

BAHMAN HAFIZI

Icarus Research, Inc.
Bethesda, Maryland

November 14, 2008

REPORT DOCUMENTATION PAGE

Form Approved
OMB No. 0704-0188

1. REPORT DATE *(DD-MM-YYYY)*	2. REPORT TYPE	3. DATES COVERED *(From - To)*
14-11-2008	Final	April 2008 – October 2008

4. TITLE AND SUBTITLE

Laser-Pumped Coherent X-Ray FEL

5a. CONTRACT NUMBER

5b. GRANT NUMBER

5c. PROGRAM ELEMENT NUMBER

6. AUTHOR(S)

Phillip Sprangle, Bahman Hafizi,* and Joseph Peñano

5d. PROJECT NUMBER
67-9466-09

5e. TASK NUMBER

5f. WORK UNIT NUMBER

7. PERFORMING ORGANIZATION NAME(S) AND ADDRESS(ES)

Naval Research Laboratory, Code 6790
4555 Overlook Avenue, SW
Washington, DC 20375

8. PERFORMING ORGANIZATION REPORT NUMBER

NRL/MR/6790--08-9163

9. SPONSORING / MONITORING AGENCY NAME(S) AND ADDRESS(ES)

Office of Naval Research
One Liberty Center
875 North Randolph Street
Arlington, VA 22203-1995

10. SPONSOR / MONITOR'S ACRONYM(S)

ONR

11. SPONSOR / MONITOR'S REPORT NUMBER(S)

12. DISTRIBUTION / AVAILABILITY STATEMENT

Approved for public release; distribution is unlimited.

13. SUPPLEMENTARY NOTES

*Icarus Research, Inc., P.O. Box 30780, Bethesda, MD 20824

14. ABSTRACT

In a laser-pumped x-ray free electron laser (FEL) an intense laser field replaces the magnetic wiggler field of a conventional FEL. Depending on the intensity and quality of both the electron beam and pump laser, the Thomson backscattered radiation can be coherently amplified. In a conventional FEL, the generation of x-rays requires electron beam energies in the multi-GeV range. In a laser-pumped x-ray FEL, electron beam energies in the multi-MeV range would be sufficient. To generate coherent x-rays with this mechanism, a number of physics and technology issues must be addressed. Foremost among these are the stringent requirements placed on the electron beam quality and brightness as well as the pump laser intensity and pulse energy. The seed radiation for the laser-pumped FEL is the laser-induced spontaneous radiation. The evolution of incoherent radiation into coherent radiation as well as the power gain lengths associated with the coherent x-rays as a function of electron beam energy spread are analyzed and discussed. There is excellent agreement between our analytical results and GENESIS simulations for the radiated power, gain length, conversion efficiency, line-width and saturation length.

15. SUBJECT TERMS

16. SECURITY CLASSIFICATION OF:			17. LIMITATION OF ABSTRACT	18. NUMBER OF PAGES	19a. NAME OF RESPONSIBLE PERSON
a. REPORT	b. ABSTRACT	c. THIS PAGE			Phillip Sprangle
Unclassified	Unclassified	Unclassified	UL	35	19b. TELEPHONE NUMBER *(include area code)* (202) 767-3493

CONTENTS

Laser-Pumped Coherent X-Ray FEL

P. Sprangle, B. Hafizi[+], and J.R. Peñano

Plasma Physics Division, Naval Research Laboratory, Washington, DC 20375
[+]Icarus Research, Inc., PO Box 30780, Bethesda, MD 20824-0780

Abstract

In a laser-pumped x-ray free electron laser (FEL) an intense laser field replaces the magnetic wiggler field of a conventional FEL. Depending on the intensity and quality of both the electron beam and pump laser, the Thomson backscattered radiation can be coherently amplified. In a conventional FEL the generation of x-rays requires electron beam energies in the multi-GeV range. In a laser-pumped x-ray FEL electron beam energies in the multi-MeV range would be sufficient. To generate coherent x-rays with this mechanism a number of physics and technology issues must be addressed. Foremost among these are the stringent requirements placed on the electron beam quality and brightness as well as the pump laser intensity and pulse energy. The seed radiation for the laser-pumped FEL is the laser-induced spontaneous radiation. The evolution of incoherent radiation into coherent radiation as well as the power gain lengths associated with the coherent x-rays are analyzed and discussed. There is excellent agreement between our analytical results and GENESIS simulations for the radiated power, gain length, conversion efficiency, line-width and saturation length. These issues, as well as others, necessary to achieve coherent amplified x-rays in a laser-pumped FEL are discussed.

Manuscript approved November 6, 2008

I. Introduction

The free-electron laser (FEL) can, in principle, generate coherent, polarized, short pulses of x-rays for numerous applications in research. There are a number of large-scale electron accelerator facilities throughout the world which will be used for x-ray generation using a conventional FEL configuration [1-4]. In a conventional FEL the electron beam propagates through a static, periodic magnetic field (wiggler) which results in stimulated emission [5-20]. Generation of x-rays at these facilities typically requires electron beam energies in the multi-GeV range with peak currents in the multi-kA range, and wiggler lengths of many tens of meters. An x-ray FEL amplifier can be operated in the self-amplified regime, eliminating the need for a coherent input x-ray source [21-26]. In this case the FEL seed radiation is provided by spontaneous incoherent emission in the wiggler.

The wiggler field in the FEL can be replaced with an electromagnetic wave such as an intense laser field. Early analysis of stimulated emission from relativistic electrons interacting with an electromagnetic pump was presented and discussed in [27]. This analysis was limited to the low-gain, thermal beam regime. In this regime the power gain lengths are extremely long making the concept impractical. The high-gain regime of the electromagnetically pumped FEL was first analyzed and discussed in [28]. In this regime the power gain lengths can be very short. However, the requirements on the electron beam quality and the pump laser power are demanding, particularly for x-ray generation. Since these early studies there have been a number of papers that have considered employing electromagnetic pumps in FELs [29-32].

In this paper we analyze and discuss a laser pumped FEL amplifier operating in the x-ray regime. The analysis considers i) electron beam thermal effects, ii) off-axis propagation and iii) the transition from incoherent (spontaneous) to coherent x-rays. The power gain length and the conversion efficiency are determined as functions of the electron beam energy spread. The radiation power as a function of interaction distance is obtained in both the incoherent and coherent regimes. The coherent power is emitted into a solid angle which is typically much greater than the solid angle associated with diffraction. For electron beams of sufficiently high quality, with energies of 7 MeV and peak currents of 500 A, we find that coherent x-rays at 15 Å can be generated with power gain lengths of $500\,\mu$m, saturation lengths of 0.4 cm and conversion efficiencies of ~ 0.01%. To achieve these values the fractional electron beam energy spread must be $\leq 0.01\%$. The pump laser for this example has a wavelength of $1\,\mu$m, pulse duration of 27 psec and power of 50 TW. To compare our results with simulations we use the GENESIS FEL code [33] and find good agreement with our analytical results. We also compare our results and GENESIS simulations for the LCLS wiggler-based FEL operating at 15Å.

II. High-Gain Regime

The laser pumped FEL is shown schematically in Fig. 1. The pump laser is taken to be circularly polarized, with normalized vector potential

$$\begin{aligned} \mathbf{a}_o(\mathbf{r},t) &= a_o\left(\cos(k_o z + \omega_o t)\hat{\mathbf{e}}_x + \sin(k_o z + \omega_o t)\hat{\mathbf{e}}_y\right) \\ &= (a_o/\sqrt{2})\exp(-i(k_o z + \omega_o t))\hat{\mathbf{e}}_\perp + c.c., \end{aligned} \tag{1}$$

where $\hat{\mathbf{e}}_\perp = (\hat{\mathbf{e}}_x + i\hat{\mathbf{e}}_y)/\sqrt{2}$ is a unit transverse vector, $\lambda_o = 2\pi c/\omega_o$ is the pump wavelength, $k_o = \omega_o/c$ is the wavenumber and $a_o = qA_o/mc^2$ is the normalized

amplitude. The pump laser power is $P_o = (m^2 c^5 / q^2)(\pi \sigma_o / \lambda_o^2) a_o^2$, where $m^2 c^5 / q^2 = 8.75\,\mathrm{GW}$, $\sigma_o = \pi r_o^2 / 2$ is the cross sectional area for a Gaussian transverse profile and r_o is the laser spot size.

The x ray radiation is given by the normalized vector potential

$$\mathbf{a}(\mathbf{r},t) = \left(a(\mathbf{r},t)/\sqrt{2}\right)\exp(i(k_z z - \omega t))\hat{\mathbf{e}}_\perp + c.c., \qquad (2)$$

where $\lambda = 2\pi c/\omega$ is the x-ray wavelength and k_z is the complex axial wavenumber.

a) 3-D Thermal Beam Dispersion Relation

Thermal effects associated with the electron beam play a critical role in the FEL interaction. The FEL dispersion relation including thermal effects is [13,15,16],

$$k_z^2 + k_\perp^2 - \frac{\omega^2}{c^2} = -8 f \frac{\nu}{r_b^2} \frac{a_o^2}{\gamma_o^3} \frac{\omega}{c} \frac{\omega_o}{c} \int_1^\infty \frac{d\gamma F_o(\gamma)}{\left[k_z + k_o - (\omega - \omega_o)/v_z + \mu k_\perp^2\right]^2}, \qquad (3)$$

where $k_\perp$ is the transverse wavenumber, f is the filling factor, i.e., ratio of electron beam to radiation beam areas, $\nu = \omega_b^2 r_b^2 / 4c^2 = N_b r_e / l_b = I_b[A]/17{,}000$ is Budker's parameter, $\omega_b = (4\pi q^2 n_b / m)^{1/2}$ is the electron beam plasma frequency, I_b is the beam current, $r_e = q^2/mc^2$ is the classical electron radius, ℓ_b is the electron bunch length, N_b is the number of electrons in a bunch, r_b is the electron beam radius and $F_o(\gamma)$ is the electron distribution function. The filling factor is a function of the interaction distance. In Eq.(3) $\mu = \gamma_{zo}^2 a_o^2 / (2\gamma_o^2 \omega / c)$ is a correction term that arises from the transverse electron motion in the field of the pump laser. The resonant frequency is a function of $k_\perp$, and for $a_o^2 << 1$ is given by

$$\omega_R(k_\perp) = \omega_{R0}(1 - (\gamma_{zo}^2 / \omega_{R0}^2) c^2 k_\perp^2), \qquad (4)$$

where the resonant frequency for on-axis ($k_\perp = 0$) propagation is

$\omega_{R0} = 4\gamma_{zo}^2 \omega_o = 4\gamma_o^2 \omega_o/(1 + a_o^2)$. The coherent radiation is emitted along the z-axis inside a narrow cone with opening angle $\theta_k = k_\perp / k_z$. The range of allowed $k_\perp$'s, i.e., emission solid angle, is important in determining the incoherent and coherent x-ray power and is discussed in Sec IIe.

i) Cold Beam

For a cold beam the electron distribution function is $F_o(\gamma) = \delta(\gamma - \gamma_o)$ and the dispersion relation is given by $D_{fel}(\mathbf{k}, \omega) = 0$ where

$$D_{fel}(\mathbf{k},\omega) = \left[k_z - \frac{\omega}{c}\left(1 - \frac{c^2 k_\perp^2}{2\omega_{R0}^2}\right)\right]\left[k_z - \frac{\omega}{c}\left(1 + \frac{(\omega - \omega_{R0})}{2\gamma_{zo}^2 \omega_{R0}} - \frac{\mu c k_\perp^2}{\omega_{R0}}\right)\right]^2 + \left(\Gamma_{go}/\sqrt{3}\right)^3. \qquad (5)$$

For a cold beam, with $k_\perp = 0$ and $\omega = \omega_{R0}$, we find $k_z = \omega/c + \Delta k$, where

$\Delta k = (1/\sqrt{3} - i)\Gamma_{go}/2$. The power growth rate as a function of ω and $k_\perp$ is

$$\Gamma_g(\omega, k_\perp) = \Gamma_{go}\left(1 - (\omega - \omega_R(k_\perp))^2/\Delta\omega^2\right), \qquad (6)$$

where the peak growth rate is $\Gamma_{go} = (5.07/\gamma_o)\left(f\nu a_o^2/(r_b^2 \lambda_o)\right)^{1/3}$, the power gain length is $L_{go} = 1/\Gamma_{go}$, and the line width associated with the power growth rate is $\Delta\omega/\omega_{R0} = (\lambda_o / L_{go})/2\pi$. As an example, the power gain length for x-rays at $\lambda = 15$ Å is shown in Fig. 2 for a cold electron beam as a function of beam current. The parameters for this plot are listed in Table I.

ii) Thermal Beam

For a thermal electron beam with distribution function

$F_o(\gamma) = (\sqrt{\pi}\,\delta\gamma)^{-1} \exp\left(-(\gamma - \gamma_o)^2/\delta\gamma^2\right)$ the dispersion relation for $k_\perp = 0$ is

$$\Delta k = \frac{\lambda_o}{4\pi}\left(\frac{\Gamma_{go}}{\sqrt{3}}\right)^3 \frac{\gamma_o}{\delta\gamma}\int_{-\infty}^{\infty} \frac{dx\,\pi^{-1/2}\,x\exp(-x^2)}{\Delta k - 2k_o(\omega-\omega_{R0})/\omega_{R0} + 4k_o(\delta\gamma/\gamma_o)x}, \qquad (7)$$

where $\delta\gamma/\gamma_o$ is the fractional energy spread. The dispersion relation can be written in the form

$$\xi = -\rho_o[1 + \{\xi + \xi_o\}Z(\xi + \xi_o)], \qquad (8)$$

where $\xi = -(\gamma_o/\delta\gamma)\Delta k/4k_o$, $\xi_o = (\gamma_o/\delta\gamma)(\omega-\omega_{R0})/2\omega_{R0}$, $\Delta k = \Delta k_r - i\Gamma_g/2$,

$\rho_o = 2.4\times10^{-5}(\lambda_o\Gamma_{go})^3(\gamma_o/\delta\gamma)^3$, $Z(\xi) \equiv \pi^{-1/2}\int_{-\infty}^{\infty} dx\exp(-x^2)/(x-\xi)$ is the plasma dispersion function and gain occurs when the imaginary part of ξ is positive. In the cold beam limit $|\xi + \xi_o| >> 1$ the dispersion relation reduces to the usual cubic equation with power growth rate given by Eq.(6) for $k_\perp = 0$ and $\xi_o = 0$.

The thermal dispersion relation can be analyzed in various limits.

In the thermal beam limit $|\xi + \xi_o| < 1$ the dispersion relation, reduces to [15]

$$\xi = -\rho_o\left(1 + i\sqrt{\pi}(\xi + \xi_o)\exp(-(\xi + \xi_o)^2)\right), \qquad (9)$$

where $Z(|\xi| < 1) = i\sqrt{\pi}\exp(-\xi^2)$. For $1 > |\xi_o| >> |\xi|$ the imaginary part of ξ is $\xi_i = -\pi^{1/2}\rho_o\xi_o\exp(-\xi_o^2)$ where $\rho_o << 1$. The maximum growth rate occurs at $\xi_o = -1/\sqrt{2}$ and is given by [15,27]

$$\Gamma_g/\Gamma_{go} = 9.1\times10^{-4}(\lambda_o\Gamma_{go})^2(\gamma_o/\delta\gamma)^2, \qquad (10)$$

where $\Gamma_{go} = (5.07/\gamma_o)\left(f\nu a_o^2/(r_b^2\lambda_o)\right)^{1/3}$ is the cold beam power growth rate and the thermal growth rate is inversely proportional to the square of the energy spread. The power growth rate at resonance ($\xi_o = 0$) in the thermal beam limit is

$$\Gamma_g / \Gamma_{go} = \frac{5.2\times10^{-8}(\lambda_o \Gamma_{go})^5 (\gamma_o / \delta\gamma)^5}{1 + 1.8\times10^{-9}(\lambda_o \Gamma_{go})^6 (\gamma_o / \delta\gamma)^6}. \quad (11)$$

In the extreme thermal limit $|\xi| << 1$ the power growth rate at resonance is given by

$$\Gamma_g / \Gamma_{go} = 5.2\times10^{-8}(\lambda_o \Gamma_{go})^5 (\gamma_o / \delta\gamma)^5. \quad (12)$$

Figure 3 plots the normalized growth rate for x-rays at $\lambda = 15\,\mathring{A}$ as a function of relative electron beam energy spread and detuning for the parameters listed in Table I. Figure 3 shows that as the energy spread of the beam is increased up to $\delta\gamma/\gamma_o \sim 5\times10^{-4}$, the FEL interaction can be detuned to increase the growth rate relative to the resonant growth rate. For a given energy spread, the optimal detuning, i.e., maximum growth rate, occurs when the difference between the beam velocity and the phase velocity of the wave is equal to the thermal velocity spread of the beam. For $\delta\gamma/\gamma_o > 5\times10^{-4}$, the growth rate is vanishingly small regardless of detuning.

b) X- Ray Conversion Efficiency

The saturated coherent power is $P_{coh,sat} = \eta N_b \gamma_o mc^2/\tau_b$, where $\eta = P_{coh,sat}/P_b$ is the conversion efficiency and $P_b = N_b \gamma_o mc^2/\tau_b = \nu \gamma_o mc^3/r_e$ is the electron beam power. The conversion efficiency in the cold beam limit can be obtained by considering the difference between the electron beam energy before and after trapping in the ponderomotive potential [17]. The efficiency at saturation is $\eta = (2/\gamma_o)(\partial\gamma_o/\partial\beta_{zo})(\beta_{zo} - \beta_{ph})$, where β_{ph} is the normalized axial phase velocity of the ponderomotive wave. From the dispersion relation the phase velocity is found to be

$v_{ph}/c = (\omega - \omega_o)/c(k_z + k_o) = \beta_{zo} - \mathrm{Re}(\Delta k)/k_z + k_\perp^2/(2k_z^2)$. The conversion efficiency at saturation, for $k_\perp = 0$, is [17]

$$\eta = 0.023(\lambda_o / L_{go}). \tag{13}$$

The x-ray conversion efficiency plotted as a function of beam current is shown in Fig. 4 for a cold electron beam along with results from GENESIS simulations. The parameters for this plot are listed in Table I. There is good agreement between theory and simulations.

c) Validity of Classical Description

The classical description is valid if the electron momentum recoil is somewhat less than the electron thermal momentum spread. In the beam frame (indicated by a prime on the variables) this condition is $\hbar k' \ll m\Delta v'$ and in the laboratory frame it can be written as [34]

$$\frac{2\gamma_o}{\sqrt{1 + a_o^2}}\left(\frac{\Delta\gamma}{\gamma_o}\right)\left(\frac{\lambda}{\lambda_c}\right) \approx \eta\gamma_o\left(\frac{\lambda}{\lambda_c}\right) > 1, \tag{14}$$

where $\lambda_c = 2\pi\hbar/mc = 0.02$ Å is the Compton wavelength,

$\Delta\gamma/\gamma_o = \gamma_o^2(1 + a_o^2)^{-1}\Delta v_z/c$ is the fractional energy spread and Δv_z is the axial velocity spread.

d) Electron Beam Quality Requirements

For high gain and efficiency the electrons must remain in phase with the ponderomotive (trapping) wave. As a result the interaction is sensitive to an axial electron velocity spread. A spread in axial electron velocity Δv_z can result in phase mixing which would reduce the gain and efficiency. The electron beam can be

considered cold, i.e., mono-energetic, provided $\Delta v_z L_{go}/c \ll \lambda$, which can be written in terms of the fractional energy spread $\Delta\gamma/\gamma \ll \lambda_o/4L_{go} \approx 10\eta$. The energy spread on the beam consists of several contributions. These contributions include: i) intrinsic energy spread, ii) transverse and longitudinal emittance, iii) space charge, iv) pump laser line width, and v) pump laser field gradients. The overall energy spread is

$$\frac{\Delta\gamma}{\gamma_o} = \left(\frac{\Delta\gamma}{\gamma_o}\right)_{\text{intrinsic}} + \left(\frac{\Delta\gamma}{\gamma_o}\right)_{\perp,\text{emit}} + \left(\frac{\Delta\gamma}{\gamma_o}\right)_{z,\text{emit}} + \left(\frac{\Delta\gamma}{\gamma_o}\right)_{\substack{\text{space}\\ \text{charge}}} + \left(\frac{\Delta\gamma}{\gamma_o}\right)_{\substack{\text{pump}\\ \text{linewidth}}} + \left(\frac{\Delta\gamma}{\gamma_o}\right)_{\substack{\text{pump}\\ \text{grad}}}, \quad (15)$$

where $(\Delta\gamma/\gamma_o)_{\perp,\text{emit}} = \varepsilon_n^2/2r_b^2 \sim 2\times10^{-4}$, $(\varepsilon_n = 1\,\text{mm}-\text{mrad},\ r_b = 50\,\mu m)$, $(\Delta\gamma/\gamma_o)_{z,\text{emit}} = \varepsilon_{n,z}^*/(\tau_b E_b) \sim 2.5\times10^{-4}$ $(\varepsilon_{n,z}^* = 25\,\text{keV}-\text{psec},\ \tau_b = 10\,\text{psec}$, and $E_b = 10\,\text{MeV})$, $(\Delta\gamma/\gamma_o)_{\substack{\text{space}\\ \text{charge}}} = \nu/\gamma_o$, $(\Delta\gamma/\gamma_o)_{\substack{\text{pump}\\ \text{linewidth}}} = \delta\lambda/2\lambda_o < 10^{-4}$. Here, ε_n is the normalized transverse emittance and $\varepsilon_{n,z}^*$ is the normalized axial emittance [35]. The energy spread contribution due to space charge leads to an energy shear which can be eliminated or substantially reduced by an appropriate tailoring of the transverse gradients of the pump laser.

The electron beam brightness $B_n = 2I_b/(\pi^2\varepsilon_n^2)$ is a measure of beam quality [35]. At the cathode the normalized brightness can be expressed as $B_n = J_c mc^2/(2\pi k_B T_c)$ where J_c is the current density at the cathode and T_c is the cathode temperature. For a photocathode with $k_B T_c = 0.1\,\text{eV}$ and $J_c = 100\,\text{A/cm}^2$ the brightness is $B_n \sim 10^8\,\text{A/(cm}-\text{rad)}^2$. The brightness needed in a laser pumped x-ray FEL is about an order of magnitude higher, i.e., $\geq 10^9\,\text{A/(cm}-\text{rad)}^2$. An axial magnetic field may be necessary to guide the electron beam though the interaction region. The

magnetic field required for a matched, i.e., constant radius, electron beam is

$B[\mathrm{kG}] = (4.7/r_b[\mathrm{cm}])(\nu/\gamma_o)^{1/2} \sim 20\mathrm{kG}$.

e) Radiation Solid Angle

The transition from spontaneous to coherent radiation is critically dependent on the angular distribution of the waves. Waves with finite $k_\perp$ have a propagation angle $\theta_k = k_\perp / k_z$ with respect to the z axis. The peak growth rate is independent of $k_\perp$ for waves propagating in the near-forward direction as indicated in Eq.(6). However, as $k_\perp$ increases the resonant frequency $\omega = \omega_R(k_\perp)$ decreases as indicated schematically in Fig.5. The minimum propagation angle is $\theta_{k,\min} = \theta_D = \lambda/\pi r_s$ where θ_D is the diffraction angle, r_s is the radial dimension of the radiation beam and $k_{\perp,\min} = 2/r_s$. In general, however, $k_\perp$ can be significantly greater than $k_{\perp,\min}$. From the power gain expression in Eq.(6), the maximum transverse wavenumber, for gain at resonance ($\omega = \omega_{R0}$), is given by

$$k_{\perp,\max} = \theta_{k,\max} k_z \approx \frac{3}{\sqrt{\pi}} \left(\frac{\lambda}{L_{go}} \right)^{1/2} k_z . \qquad (16)$$

The ratio of the maximum to minimum transverse wavenumbers is $k_{\perp,\max}/k_{\perp,\min} \approx 3(Z_R/L_{go})^{1/2}$ where $Z_R = \pi r_s^2/\lambda$ is the Rayleigh length. For a laser pumped FEL, $Z_R >> L_{go}$. In the case of an optically guided FEL amplifier $Z_R \approx L_{go}$. Other processes, such as the electron transverse wiggle and betatron oscillations, can also limit the range of transverse wavenumbers.

The solid angle associated with the radiation beam is $\Delta\Omega_k = \pi\theta_{k,\max}^2$ where $\theta_{k,\max} = k_{\perp,\max}/k_z$. The spontaneous (incoherent) radiation is directed into a forward cone with angle $\theta_{incoh} \approx 1/\gamma_{zo}$ [36] which is typically much greater than $\theta_{k,\max}$. In the start-up regime the propagation angle $\theta_{k,\max}$ determines the portion of the spontaneous power that is within the gain spectrum and amplified as shown schematically in Fig.5.

III. Transition from Incoherent to Coherent Radiation

The discrete nature of the electron beam interacting with the pump laser field leads to the generation of spontaneous (incoherent) radiation that can be subsequently amplified [21-26]. During amplification, however, there is an increase in the coherence of the radiation.

The wave equation governing the x-ray generation is $\left(\nabla^2 - c^{-2}\partial^2/\partial t^2\right)\mathbf{E}(\mathbf{r},t) = 4\pi c^{-2} g(z)\partial\mathbf{J}(\mathbf{r},t)/\partial t + 4\pi\, g(z)\nabla\rho(\mathbf{r},t)$ where the field and current density are $\mathbf{E}(\mathbf{r},t), \mathbf{J}(\mathbf{r},t) = (E(\mathbf{r},t), J(\mathbf{r},t))\hat{\mathbf{e}}_\perp + c.c.$, $\rho(\mathbf{r},t)$ is the charge density and $g(z) = 1$ for $0 \le z \le \bar{z}$ defines the interaction region and is zero otherwise. The driving current density consists of a coherent and an incoherent (discrete) component

$$\begin{aligned}\mathbf{J}(x,y,z,t) &= q\sum_{i=1}^{N_b} \tilde{\mathbf{v}}_i(t)\delta(x-\tilde{x}_i(t))\delta(y-\tilde{y}_i(t))\delta(z-\tilde{z}_i(t)) \\ &= \mathbf{J}_{coh}(\mathbf{r},t) + q\sum_{i=1}^{N} \tilde{\mathbf{v}}_i^{(o)}(\mathbf{r}_o,\mathbf{v}_o,t)\delta(\mathbf{r}-\tilde{\mathbf{r}}_i^{(o)}(t)),\end{aligned} \tag{17}$$

where $\tilde{\mathbf{r}}_i^{(o)}(t)$, $\tilde{\mathbf{v}}_i^{(o)}(t)$ are the unperturbed electron trajectories given by $\tilde{\mathbf{v}}^{(o)} = (-c\mathbf{a}_o/\gamma_o, \mathrm{v}_{zo})$, $\mathbf{J}_{coh}(\mathbf{r},t)$ is the coherent current density which is responsible for the FEL interaction and the summation term in Eq.(17) is responsible for spontaneous

emission. Substituting the current density, Eq.(17), into the wave equation and Fourier transforming the spatial and temporal variables we obtain,

$$D(\mathbf{k},\omega)\hat{E}(k_x,k_y,k_z,\omega) = \frac{1}{8\pi^2}\left(\frac{4\pi q}{c}\right)\frac{a_o}{\sqrt{2}}\frac{i}{\gamma_o}\bar{z}\exp\left(iK(k_z,\omega)\bar{z}/2\right)\left(\frac{\sin(K(k_z,\omega)\bar{z}/2)}{K(k_z,\omega)\bar{z}/2}\right)\sum_{i=1}^{N_b}\exp(i\chi_{o,i}), \tag{18}$$

where $K(k_z,\omega) = (\omega-\omega_o)/\mathrm{v}_{zo} - (k_z+k_o)$, $\chi_{o,i} = -k_x x_{o,i} - k_y y_{o,i} + (\omega-\omega_o)t_{o,i}$ and the charge density has been neglected [23]. In obtaining Eq.(18) harmonics are neglected since we assumed $k_\perp|\delta x| << 1$, where $|\delta x| = a_o/(2\gamma_o k_o)$ is the magnitude of the electron transverse wiggle motion in the pump laser.

The function $D(\mathbf{k},\omega)$ is given by

$$\begin{aligned} D(\mathbf{k},\omega) &= -\frac{D_{fel}(\mathbf{k},\omega)}{\left(k_z - (\omega/c)\left(1+(\omega-\omega_{R0})/(2\gamma_{zo}^2\omega_{R0})\right)\right)^2} \\ &= -\frac{(k_z-k_1(k_\perp,\omega))(k_z-k_2(k_\perp,\omega))(k_z-k_3(k_\perp,\omega))}{(k_z+k_o-(\omega-\omega_o)/\mathrm{v}_{zo})^2}, \end{aligned} \tag{19}$$

where the roots of the dispersion relation are denoted by k_1, k_2, k_3 and k_1 denotes the growing root. Solving the wave equation for the field associated with the growing root, i.e., integrating around the pole at $k_z = k_1(k_\perp,\omega)$, yields

$$\begin{aligned} \hat{E}(k_\perp,z,\omega) = \frac{1}{2(\pi)^{1/2}}\frac{q}{c}\frac{a_o}{\gamma_o}\bar{z}\exp\left(iK_1\bar{z}/2\right)\left(\frac{\sin(K_1\bar{z}/2)}{K_1\bar{z}/2}\right)\times \\ G(k_1,k_\perp,\omega)\exp(ik_1(k_\perp,\omega)z)\sum_{i=1}^{N_b}\exp(i\chi_{o,i}), \end{aligned} \tag{20}$$

where $K_1 = K(k_1,\omega) = (\omega-\omega_o)/\mathrm{v}_z - (k_1+k_o) = [\omega-\omega_{R0}(1-\gamma_{zo}^2 c^2 k_\perp^2/\omega_{R0}^2)]/(2c\gamma_{zo}^2)$ .and

$G(k_1,k_\perp,\omega) = ((k_1+k_o-(\omega-\omega_o)/\mathrm{v}_{zo})^2)/(k_1-k_2(k_\perp,\omega))(k_1-k_3(k_\perp,\omega))$.

The intensity is given by $I(r,z,t) = (c/2\pi)\left\langle E(r,z,t)E^*(r,z,t)\right\rangle$ where $\langle\ \rangle$ denotes an average over electrons. If the electrons are initially randomly distributed, we use the fact that $\left\langle \sum_{i=1}^{N_b} \exp(i\chi_{o,i}) \sum_{j=1}^{N_b} \exp(-i\chi_{o,j}) \right\rangle = N_b$ and obtain

$$\left\langle \hat{E}(r,z,\omega)\hat{E}^*(r,z,\omega)\right\rangle = \frac{1}{4\pi}\frac{q^2}{c^2}\frac{a_o^2}{\gamma_o^2} N_b \times$$
$$\left| \int_0^\infty k_\perp\, dk_\perp\, z \exp\left(i\frac{K_1 z}{2}\right)\left(\frac{\sin(K_1 z/2)}{K_1 z/2}\right) G(k_1,k_\perp,\omega)\, J_o(k_\perp r) \exp(i\, k_1(k_\perp,\omega)\, z)\right|^2, \tag{21}$$

where we have set $\bar{z} = z$. The spectral power, defined by

$$\frac{d\hat{P}}{d\omega} = \int d\Omega_k \left(\frac{d^2\hat{P}}{d\omega d\Omega_k}\right) = \frac{c}{\tau_b}\int_0^\infty r dr \left\langle \hat{E}(r,z,\omega)\hat{E}^*(r,z,\omega)\right\rangle, \tag{22}$$

is given by

$$\frac{d^2\hat{P}}{d\omega d\Omega_k} = 8\nu\gamma_o^2 mc^2 \left(\frac{z}{\lambda_o}\right)^2 \left(\frac{a_o}{1+a_o^2}\right)^2 \times$$
$$\left|\exp(i K_1 z/2)\right|^2 \left|\frac{\sin(K_1 z/2)}{K_1 z/2}\right|^2 \left|G(k_1 k_\perp,\omega)\right|^2 \left|\exp(i\, k_1(k_\perp,\omega)\, z)\right|^2, \tag{23}$$

where $k_\perp\, dk_\perp = (k_z^2/2\pi)d\Omega_k$, $d\Omega_k$ is the differential solid angle associated with the wave vector and the relation $\int_0^\infty r dr\, J_o(k_\perp r)\, J_o(k'_\perp r) = \delta(k_\perp - k'_\perp)/k_\perp$ was used.

a) Incoherent Radiation

The spectral brightness in the absence of the FEL interaction is the spontaneous (incoherent) spectral brightness and is obtained from Eq.(23) by setting $k_1 = (\omega/c)(1 - c^2 k_\perp^2/2\omega_R^2)$, together with

$\left|\exp(i K_1 z/2)\right|^2 = \left|G(k_1, k_\perp, \omega)\right|^2 = \left|\exp(i k_1(k_\perp, \omega) z)\right|^2 = 1$. The incoherent spectral brightness is

$$\left(\frac{d^2 \hat{P}_{incoh}}{d\omega\, d\Omega_k}\right) = 8\nu\gamma_o^2 mc^2 \left(\frac{z}{\lambda_o}\right)^2 \left(\frac{a_o}{1+a_o^2}\right)^2 \left|\frac{\sin(K_1 z/2)}{K_1 z/2}\right|^2 . \tag{24}$$

The incoherent power radiated by the electron bunch per unit solid angle is

$$\frac{dP_{incoh}}{d\Omega_k} = \int_0^\infty d\omega \left(\frac{d^2 \hat{P}_{incoh}}{d\omega d\Omega_k}\right) = 4\pi\gamma_o^2 \frac{\nu mc^3}{\lambda} \frac{z}{\lambda_o} \left(\frac{a_o}{1+a_o^2}\right)^2 . \tag{25}$$

The incoherent power within the solid angle $\Delta\Omega_{incoh}$ is

$$P_{incoh}(z) = 16\pi\gamma_o^3 \frac{a_o^2}{(1+a_o^2)^3} \frac{r_e}{\lambda_o} \frac{z}{\lambda_o} \Delta\Omega_{incoh} P_b , \tag{26}$$

where $\Delta\Omega_{incoh} \le \pi/\gamma_{zo}^2$ is the solid angle associated with the incoherent radiation and $P_b = \nu\gamma_o mc^3/r_e$ is the electron beam power.

b) Coherent Radiation

A small portion of the spontaneous radiation spectrum overlaps the gain spectrum and is amplified as depicted in Fig. 5. The coherently amplified portion of the spectrum is determined by the relative line widths of the spontaneous and gain spectra, as well as the range of amplified transverse wave numbers $k_\perp$ given by Eq.(16). The fractional line widths associated with the coherent and incoherent (spontaneous) power spectrum are respectively

$$\delta\omega_{coh}(z)/\omega_{R0} = (1/2\pi)(\lambda_o/L_{go})\sqrt{L_{go}/z} , \tag{27a}$$

and

$$\delta\omega_{incoh}(z)/\omega_{R0} = (1/2)(\lambda_o/z) . \tag{27b}$$

The ratio of the linewidths is $\delta\omega_{coh}/\delta\omega_{incoh} = (1/\pi)\sqrt{z/L_{go}}$ which implies that for interaction distances less than ~ $10L_{go}$, the coherent power spectrum is narrower than the spontaneous spectrum. For $z > L_{go}$, we find that $\left|\exp(iK_1 z/2)\right|^2 \left|\sin(K_1 z/2)/(K_1 z/2)\right|^2 \approx (2L_{go}/z)^2$, and the coherent power spectral brightness in Eq. (23) is

$$\frac{d^2\hat{P}_{coh}}{d\omega d\Omega_k} = (32/9)\nu\gamma_o^2 mc^2\left(\frac{z}{\lambda_o}\right)^2\left(\frac{a_o}{1+a_o^2}\right)^2\left(\frac{L_{go}}{z}\right)^2\exp\left(\Gamma_g(\omega,k_\perp)z\right), \qquad (28)$$

where we used $\left|G(k_1,k_\perp,\omega)\right|^2 = 1/9$, i.e., 1/9 of the incoherent power is available for gain. Using the power growth rate spectrum in Eq.(6), Eq.(28) can be integrated over frequency to give

$$\frac{dP_{coh}}{d\Omega_k} = 6.3\nu\gamma_o^2 mc^2\left(\frac{z}{\lambda_o}\right)^2\left(\frac{a_o}{1+a_o^2}\right)^2\left(\frac{L_{go}}{z}\right)^2\left(\Delta\omega\sqrt{\frac{L_{go}}{z}}\right)\exp\left(\Gamma_{go}z\right), \qquad (29)$$

where $\Delta\omega/\omega_{R0} = (\lambda_o/L_{go})/2\pi$.

The coherent radiation beam is confined to a narrow forward cone with solid angle $\Delta\Omega_k = \pi\theta_{k,\max}^2$ where $\theta_{k,\max}$ is given by Eq.(16). The incoherent radiation, on the other hand, is confined to a cone angle $\theta_{incoh} \approx 1/\gamma_{zo} > \theta_{k,\max}$.

The integration over solid angle in Eq.(29) can be approximated by evaluating the integrand at $k_\perp = 0$ and multiplying by the solid angle $\Delta\Omega_k$. The coherent power is given by

$$P_{coh}(z) = 25\gamma_o^3\frac{a_o^2}{(1+a_o^2)^3}\left(\frac{L_{go}}{\lambda_o}\right)\left(\frac{r_e}{\lambda_o}\right)\left(\frac{L_{go}}{z}\right)^{1/2}\Delta\Omega_k P_b\exp\left(z/L_{go}\right). \qquad (30)$$

The coherent power in Eq.(30) will be compared with GENESIS simulations in the x-ray regime.

For interaction distances much greater than a Rayleigh length, but shorter than the saturation length, $L_{sat} > z >> Z_R$ the propagation angle is equal to the diffraction angle, i.e., $\theta_k = \theta_D$ and the coherent power from Eq.(30) becomes

$$P_{coh}(z >> Z_R) = 0.01\eta\gamma_o mc^2\left(\frac{z}{L_{go}}\right)^2\left(\frac{r_b^2/r_s^2}{f}\right)\delta\omega_{coh}(z)\exp\left(z/L_{go}\right), \qquad (31)$$

where $\delta\omega_{coh}(z)/\omega_{R0} = (\Delta\omega/\omega_{R0})\sqrt{L_{go}/z} = 6.9\eta\sqrt{L_{go}/z}$, $\eta = 0.023(\lambda_o/L_{go})$ is the conversion efficiency and f is the filling factor. The coherent power in this limit, Eq.(31) is similar in form to that given in [21,23,24]. The ratio of the coherent power to the incoherent power for the same solid angle and for $z > L_{go}$ is

$$\left(\frac{P_{coh}}{P_{incoh}}\right)_{\Delta\Omega_k} = 1.6\left(\frac{L_{go}}{z}\right)^2\frac{\delta\omega_{coh}(z)}{\delta\omega_{incoh}(z)}\exp(z/L_g) = \frac{1}{2}\left(\frac{L_{go}}{z}\right)^{3/2}\exp(z/L_{go}). \qquad (32)$$

c) Saturation Length and Line Width

The saturation length for the coherent radiation can be obtained by setting P_{coh} in Eq.(30) equal to the conversion efficiency times the electron beam power, ηP_b, where η is given by Eq.(13). The number of power gain lengths at saturation, $N_{sat} = L_{sat}/L_{go}$, is given by

$$N_{sat}^{-1/2}\exp(N_{sat}) = 9.2\times10^{-4}\left(\frac{\lambda_o}{L_{go}}\right)^2\left(\frac{\lambda_o}{r_e}\right)\frac{(1+a_o^2)^3}{a_o^2}\frac{1}{\gamma_o^3\Delta\Omega_k}. \qquad (33)$$

The fractional line width associated with the coherent radiation, for $k_\perp \sim 0$, at saturation is

$$\frac{\delta\omega_{coh}}{\omega_{R0}} = N_{sat}^{-1/2}\frac{\Delta\omega}{\omega_{R0}} = \frac{N_{sat}^{-1/2}}{2\pi}\frac{\lambda_o}{L_{go}}. \tag{34}$$

There is an additional contribution to the line width due to the finite transverse wavenumber, $k_\perp$, spectrum which is given by $\gamma_{zo}^2\theta_k^2$, as indicated in Eq.(4).

IV. Comparison of Theory with Simulations

In this section we compare the analytical result for the coherent power, Eq.(30), with the simulation results from GENESIS [33]. GENESIS simulates the conventional wiggler based FEL amplifier, including start-up. In using GENESIS to stimulate the laser pumped FEL, the wiggler period in GENESIS is set equal to twice the pump laser wavelength $\lambda_w = \lambda_o/2 = 0.5\mu\text{m}$, and the wiggler transverse gradients are removed. Besides GENESIS there are other FEL simulation codes that can be used to simulate the FEL start-up physics [37]. Before discussing an example of an x-ray laser pumped FEL it is useful to consider the application of the theory to a conventional FEL operating in the x-ray regime. For this comparison we use the Linac Coherent Light Source (LCLS) FEL at SLAC [1].

a) Wiggler based X-Ray FEL

The parameters of the LCLS FEL operating at 15 Å are given in Table II. In the GENESIS simulations we use a circularly polarized wiggler and a cold electron beam to make a comparison with theory. The wiggler strength parameter is therefore smaller by a factor of $\sqrt{2}$ than the actual value used in the original LCLS design [1]. Figure 6 plots the power as a function of propagation distance within the wiggler. The blue curve is the result of a Genesis simulation. The dashed curve and solid black curves represent the theoretically calculated incoherent and coherent power, respectively. The theoretical

incoherent and coherent power are functions of the maximum solid angle as indicated by Eqs. (26) and (30). In calculating the theoretical incoherent power, we assume a maximum solid angle of $\Delta\Omega_{incoh} = \pi/(3\gamma_{zo})^2$. For the coherent power, we used the maximum solid angle given by Eq. (16) and a gain length consistent with the GENESIS simulation. The red curve represents the total theoretical power at a given interaction length. There is excellent agreement between theory and simulation in both the incoherent ($z < 7$ m) and coherent ($z > 7$ m) regimes.

Figure 7a plots the radiation intensity profile at saturation and shows that it is highly localized to region of the electron beam. Figure 7b shows the distribution of power over transverse wave-number, i.e., $dP/dk_{\perp}$. Consistent with Eq. (16), most of the power is contained with the angle $\theta_{k,\max}$, which in this case is ~ 20 times larger than the diffraction angle.

b) Laser Pumped X-Ray FEL

The parameters used in the laser pumped FEL are listed in Table I. For these parameters lethargy effects (electron beam slippage) are negligible. Figure 8 shows the evolution of the x-ray power as a function of interaction length. The theoretically calculated incoherent and coherent powers are shown separately. In this parameter regime, the maximum transverse resolution of the simulation is not sufficient to resolve the maximum propagation angle given by Eq. (16). Hence, in calculating the theoretical incoherent and coherent power for comparison with the simulations, the maximum angle is taken to be $\theta_{sim} = \lambda/(2\Delta_x)$, i.e., the maximum angular resolution of the simulation, where Δ_x is the transverse grid size. The transition from incoherent to coherent radiation

occurs after ~ 2-3 power gain lengths. The power gain length is $L_{go} = 500\mu m$ while the saturation length is $L_{sat} = 8L_{go} = 0.4cm$. The conversion efficiency is $\eta = 0.01\%$ which corresponds to a saturated coherent x-ray power of $P_{coh} = 340kW$. The theoretical conversion efficiency, in Eq.(13), gives a value of 0.01% in excellent agreement with the GENESIS simulations.

Figure 9a plots the transverse x-ray intensity profile at saturation and shows that the radiation is highly localized to the electron beam and contains a large number of higher order transverse modes. Figure 9b plots the distribution of power over transverse wavenumber and shows there is significant power over the entire wave-number range resolved by the simulation.

In this example the required relative electron beam energy spread is $\leq 0.01\%$. Higher electron beam energy spreads would substantially reduce the lasing efficiency and limit the growth of coherent x-ray power. This example indicates the stringent requirements placed on both the electron beam and pump laser.

V. Conclusions

We have analyzed a high-gain, laser pumped, x-ray FEL amplifier. The analysis includes i) electron beam thermal effects, ii) off-axis propagation and iii) the transition from incoherent to coherent x-rays. The power gain length, saturation length, line-width and conversion efficiency have been calculated for the laser pumped FEL. We find there is good agreement between our theoretical results and GENESIS simulations. For electron beams of sufficiently high quality, with energies of $7MeV$ and currents of $500A$, we find that coherent x-rays at 15 Å can be generated with power gain lengths of $500\mu m$, saturation lengths of $0.4cm$ and conversion efficiencies of 0.01%. To achieve

these values the fractional electron beam energy spread must be $< 0.01\%$. The pump laser energy per pulse is ~ 500 J. While such a coherent x-ray source would have a number of attractive features, the requirements placed on both the electron beam and pump laser are challenging.

Acknowledgements: This work was supported by NRL and ONR.

References

1. Linac Coherent Light Source Conceptual Design Report, SLAC-R-593, UC-414, SLAC, 2002.

2. TESLA Technical Design Report, TESLA FEL 2002-09, DESY, 2002.

3. SPring-8 Compact SASE Source Conceptual Design Report, http://www.xfel.spring8.or.jp (2005).

4. I. S. Ko, in *Proceedings of the 2005 Free Electron Laser Conference* (Stanford, CA, USA, 2005), p. 216.

5. T.C. Marshall, *Free-electron lasers*. New York, NY, USA: Macmillan, 1985.

6. C.A. Brau, *Free-electron lasers*. San Diego, CA, USA: Academic, 1990.

7. H.P. Freund and T.M. Antonsen, *Principles of free-elelctron lasers*. London, UK: Chapman & Hall, 1992.

8. W. B. Colson, Nucl. Instrum. Methods Phys. Research A, vol. 237, pp. 1-9, 1985.

9. C.W. Roberson and P. Sprangle, Phys. Fluids, vol. 1, pp. 3-42, 1989.

10. P.G. O'Shea and H.P. Freund, Science, vol. 292, pp. 1853-1858, 2001.

11. P. Sprangle, J. Plasma Phys., vol. 11, pp. 299-309, 1974.

12. L.R. Elias, W.M. Fairbank, J.M.J. Madey, H. A. Schwettman and T.I. Smith, Phys. Rev. Lett., vol. 36, pp. 717-720, 1976.

13. N.M. Kroll and W.A. McMullin, Phys. Rev. A, vol.17, pp. 300-308, 1978.

14. A.A. Kolomenskii and A.N. Lebedev, Sov. J. Quantum Electron., vol. 8, pp. 879-884, 1978.

15. P. Sprangle and A. T. Drobot, J. Appl. Phys., vol. 50, pp.2652-2661, 1979.

16. P. Sprangle and R.A. Smith, Phys. Rev. A, vol. 21, pp. 293-301, 1980.

17. P. Sprangle, C.M. Tang and W.M. Manheimer, Phys. Rev. A, vol. 21, pp. 302-318, 1980.

18. N.M. Kroll, P.L. Morton and M.N. Rosenbluth, IEEE J. Quantum Electron., vol. QE-17, pp. 1436-1468, 1981.

19. D. Prosnitz, A. Szoke and V.R. Neil, Phys. Rev. A, vol. 24, pp. 1436-1451, 1981.

20. R. Bonifacio, C. Pellegrini, L. Narducci, Opt. Commun., vol. 50, pp. 373-378, 1985.

21. K.J. Kim, Phys. Rev. Lett., vol. 57, pp. 1871-1874, 1986.

22. C. Pellegrini, Nucl. Instrum. Methods Phys. Research, vol. A 445, pp. 124-127, 2000.

23. Z. Huang and K.J. Kim, Nucl. Instrum. Meth. Phys. Research A, vol. 507, pp.65-68, 2003.

24. Z. Huang and K.J. Kim, Phys. Rev. ST Accel. Beams, vol. 10, pp. 034801-26, 2007.

25. J.B. Murphy and C. Pellegrini, J. Opt. Soc. Am. B **2**, 259 (1985).

26. N. Piovella, Phys. Plasmas **6**, 3358 (1999).

27. R.H. Pantell, G. Soncini and H.E. Puthoff, IEEE J. Quantum Electron., vol. QE-4, pp. 905-907, 1968.

28. P. Sprangle and V.L. Granatstein, Appl. Phys. Lett., vol. 25, pp.377-379, 1974.

29. J. Gea-Banacloche, G.T. Moore, R.R. Schlicher, M.O. Scully and H. Walther, IEEE J. Quantum Electron., vol. QE-23, pp. 1558-1570, 1987.

30. P. Sprangle, B. Hafizi and F. Mako, Appl. Phys. Lett., vol. 55, pp. 2559-2560, 1989.

31. D.F. Gordon, P. Sprangle, B. Hafizi and C.W. Roberson, Nucl. Instrum. Methods Phys. Research A, vol. 475, pp. 190-194, 2001.

32. A. Bacci, M. Ferrario, C. Maroli, V. Petrillo and L. Serafini, Phys. Rev. ST. Accel. Beams **9**, 060704 (2006).

33. S. Reiche, Nucl. Instrum. Methods Phys. Research A, vol. 429, pp. 243-248, 1999.

34. R. Bonifacio, Nucl. Instrum. Methods Phys. Research A, vol. 546, pp. 634-638, 2005.

35. M. Reiser, *Theory and Design of Charged Particle Beams.* Berlin, Germany: Wiley-VCH, 2008.

36. E. Esarey, S.K. Ride and P. Sprangle, Phys. Rev. E, vol. 48, pp. 3003-3021, 1993.

37. W.M. Fawley, Nucl. Instrum. Methods Phys. Research A, vol. 507, pp. 19-25, 2003.

Electron Beam Parameters	
Energy	$E_b = 7\,\text{MeV}\ (\gamma_o = 14.5)$
Current	$I_b = 500\,\text{A}$
Radius	$r_b = 70\,\mu\text{m}$
Energy spread limit	$\Delta\gamma/\gamma \le \eta = 0.01\%$
Pump Laser Parameters	
Wavelength	$\lambda_o = 1\,\mu\text{m}$
Strength	$a_o = 0.5$
Power	$P_o = 17\,\text{TW}$
Energy/pulse	$E_o = P_o \tau_L = 450\,\text{J}$
Pulse duration	$\tau_L = 2L_{sat}/c = 27\,\text{psec}$
X-Ray Parameters	
Wavelength	$\lambda = 15\,\text{Å}$
Spot size (at saturation)	$r_s = 70\,\mu\text{m}$
Rayleigh length (at saturation)	$Z_R = 10\,\text{m}$
Power gain length	$L_{go} = 500\,\mu\text{m}$
Conversion efficiency	$\eta = 0.01\%$
Saturation length	$L_{sat} = 0.4\,\text{cm}$
Saturated power	$P_{sat} = 340\,\text{kW}$

Table I. Parameters for a Laser Pumped-FEL

Electron Beam Parameters	
Energy	$E_b = 4.52\text{GeV}$ ($\gamma_o = 8.9\times10^3$)
Current	$I_b = 3.4\text{kA}$
Radius	$r_b = 80\mu\text{m}$
Energy spread limit	$\Delta\gamma/\gamma \le \eta = 0.08\%$
Wiggler (Circular) Parameters	
Period	$\lambda_w = 3\text{cm}$
Strength	$a_w = 2.62$
X-Ray Parameters	
Wavelength	$\lambda = 15\text{Å}$
Spot size (at saturation)	$r_s = 140\mu\text{m}$
Rayleigh length (at saturation)	$Z_R = 42\text{m}$
Power gain length	$L_{go} = 2\text{m}$
Conversion efficiency	$\eta = 0.08\%$
Saturation length	$L_{sat} = 28\text{m}$
Saturated power	$P_{sat} = 12.5\text{GW}$

Table II. Parameters for LCLS FEL. Note that the actual LCLS wiggler is linearly polarized with $a_w = 3.7$.

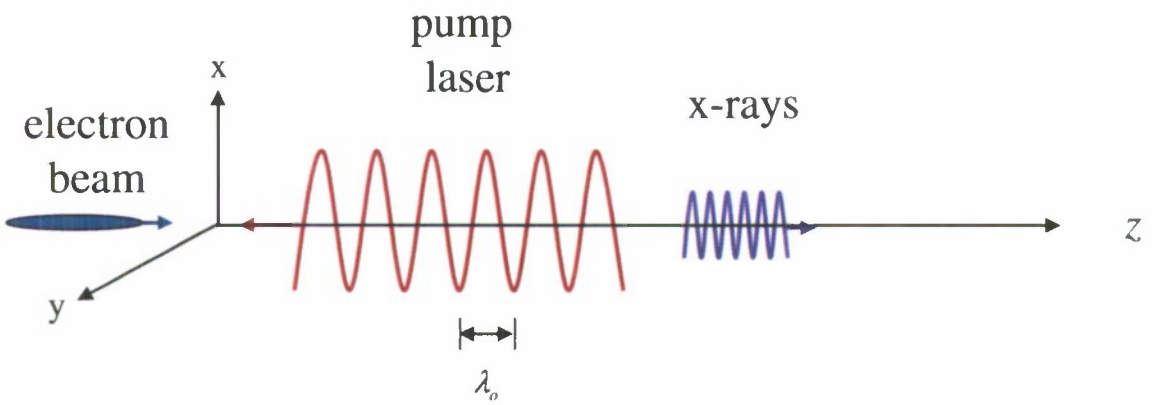

Figure1: Schematic of laser-pumped free-electron laser. The pump laser and electron beam propagate in opposite directions along the z axis.

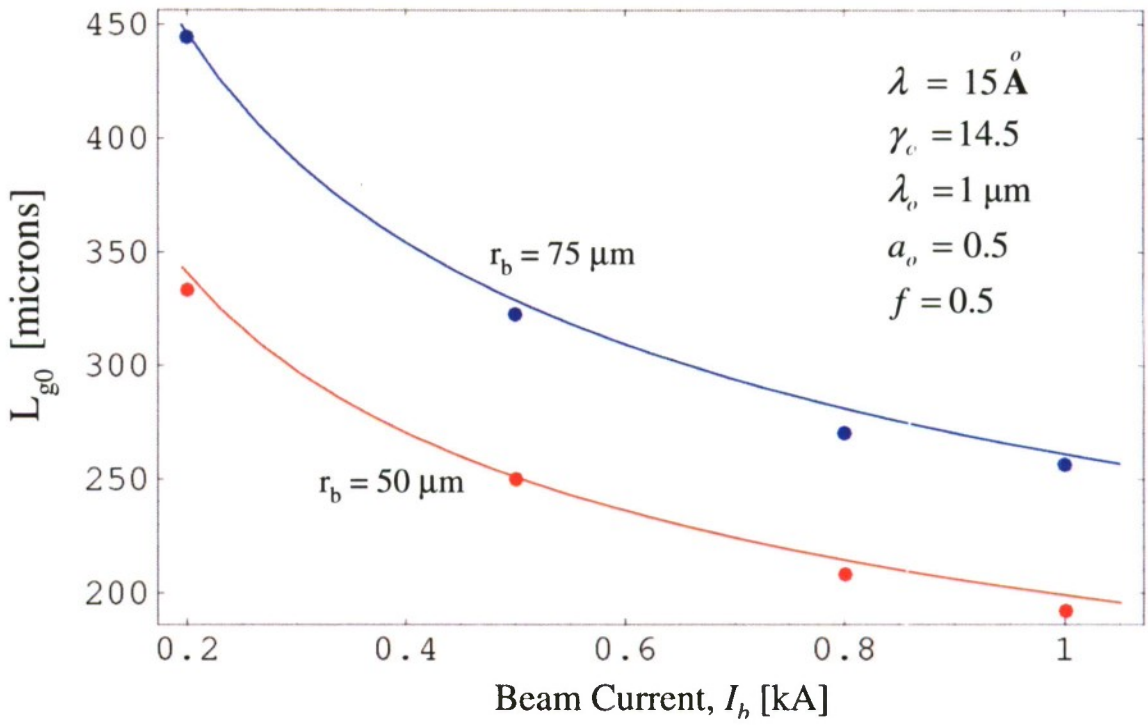

Figure 2: X-ray (λ=15 Å) power gain length L_{go} versus beam current for a cold electron beam with electron beam radius r_b=50μm (red) and r_b=75μm (blue). The curves are from Eq. (6) with $L_{go} = 1/\Gamma_{go}$ and the solid circles are from GENESIS simulations. The other parameters are, a_o=0.5, λ_o=1μm and E_b=7 MeV .

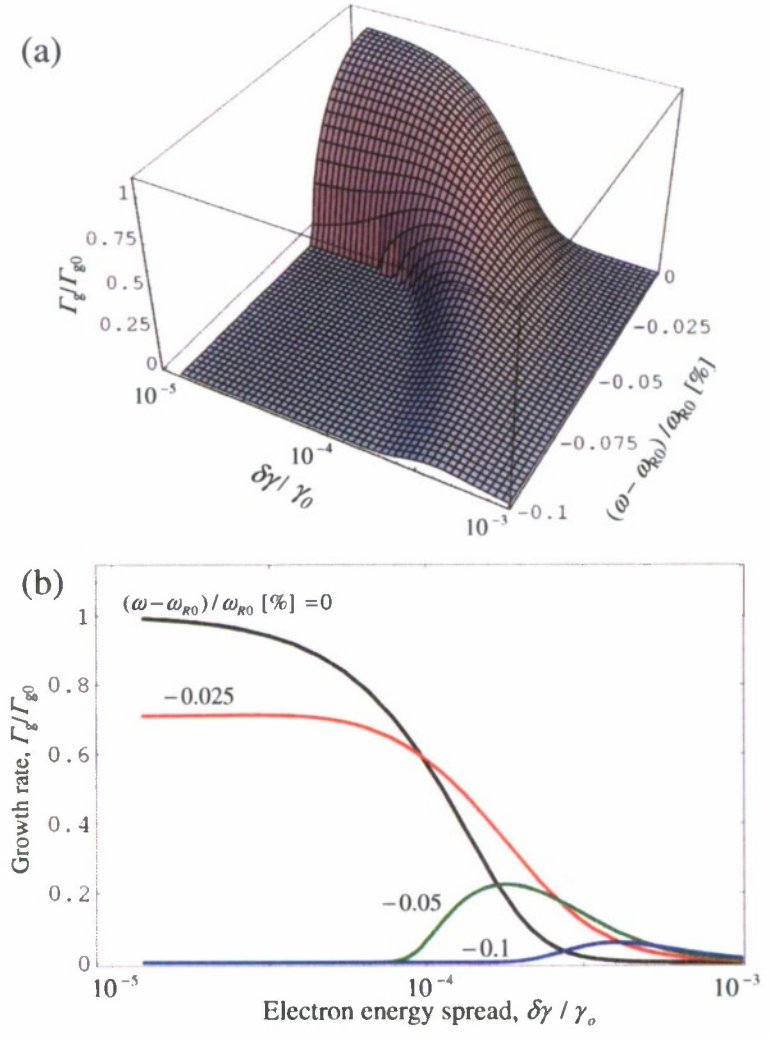

Figure 3: (a) Surface plot of normalized x-ray growth rate Γ_g/Γ_{g0} from Eq. (8) versus fractional electron beam energy spread $\delta\gamma/\gamma_o$ and fractional detuning $(\omega-\omega_{R0})/\omega_{R0}$ for the parameters of the laser-pumped FEL of Table I. (b) Line plots of Γ_g/Γ_{g0} versus $\delta\gamma/\gamma_o$ for various values of detuning for the same data as shown in Fig. 3a.

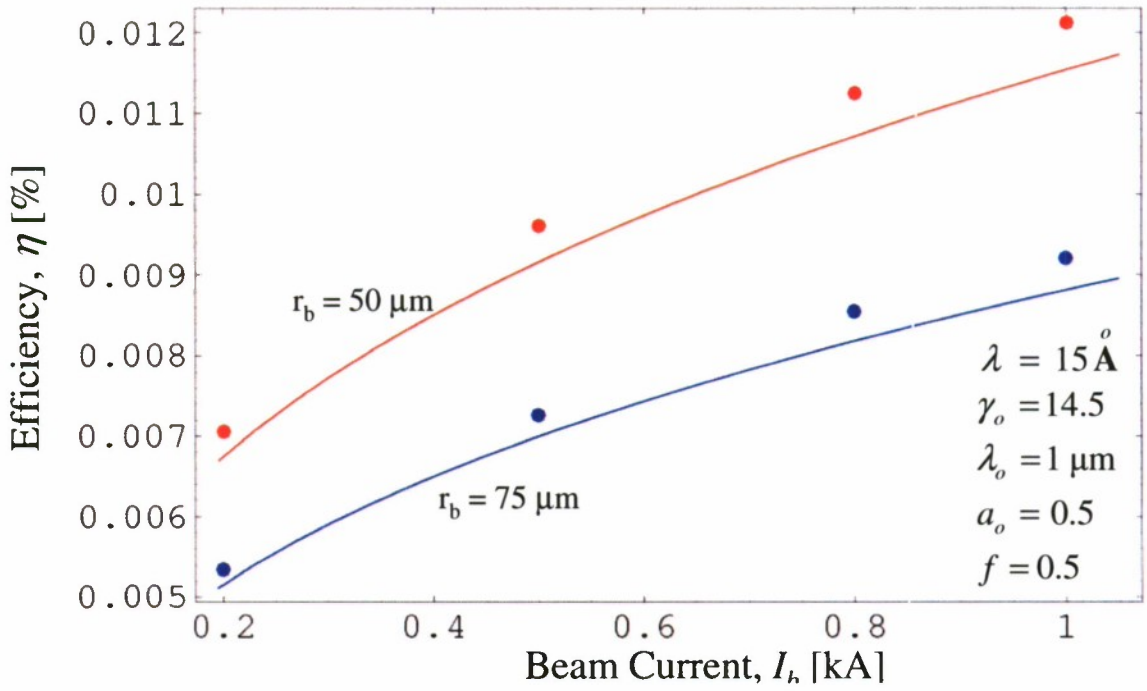

Figure 4: X-ray conversion efficiency versus beam current for a cold electron beam, with electron beam radius $r_b = 50\mu m$ (red) and $r_b = 75\mu m$ (blue). The curves are from Eq.(13) and the solid circles are from GENESIS simulations. The parameters are the same as in Fig. 2.

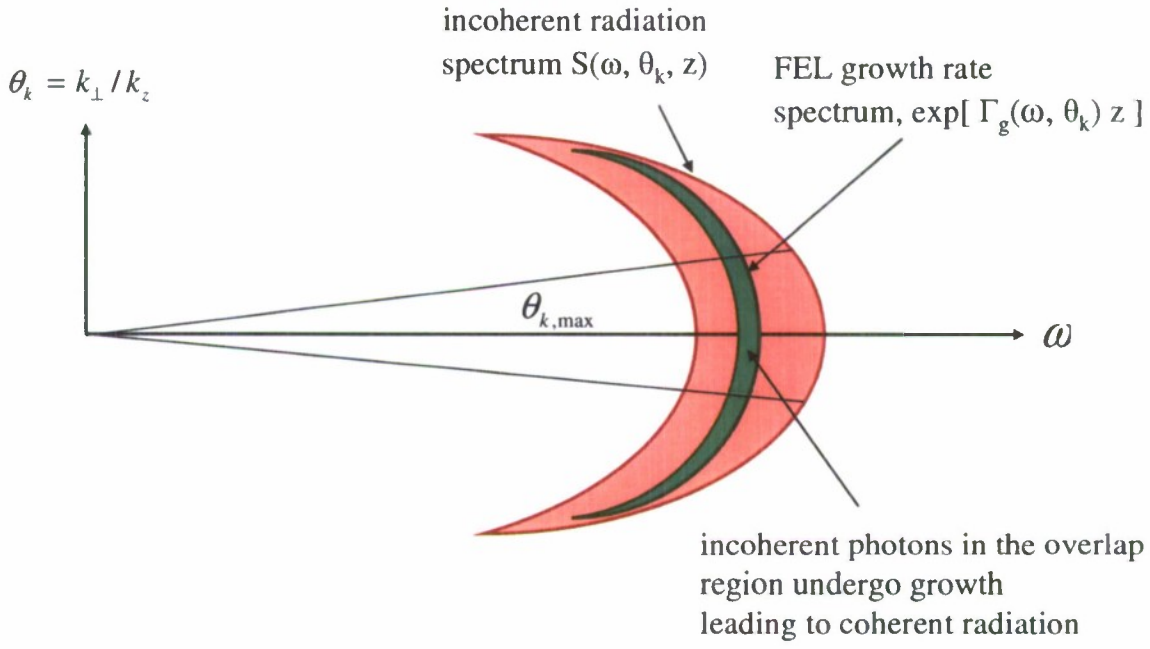

Figure 5: Schematic diagram of the incoherent (spontaneous) and coherent (growth rate) spectrum in the $(\omega, k_\perp / k_z)$ plane showing the region of overlap. The red area corresponds to the region of incoherent emission of radiation from the electron beam interacting with the pump laser. The green area indicates the growth rate spectral region in which the radiation grows exponentially.

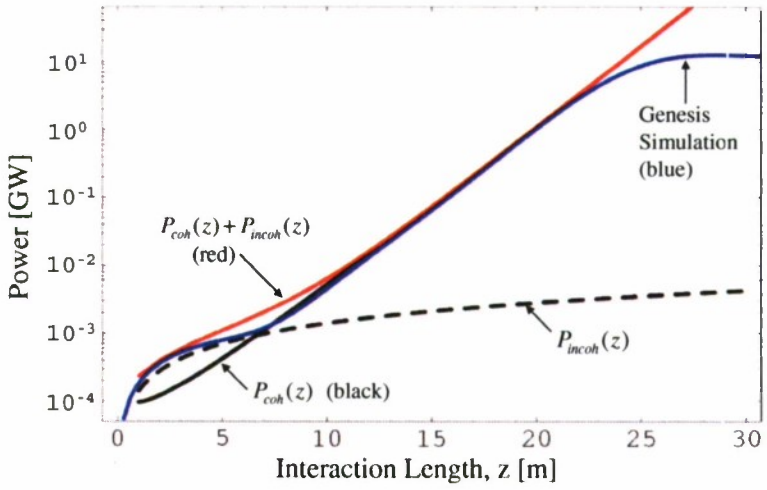

Figure 6: Power versus interaction length for the LCLS FEL (cold beam) with parameters listed in Table II. Curves denote coherent power (solid black), incoherent power (dashed), total theoretical power (red), and the result of a Genesis simulation (blue). The theoretical efficiency is $\eta = 0.023(\lambda_o / L_{go}) = 0.1\%$. The efficiency observed in the GENESIS simulation is 0.08%.

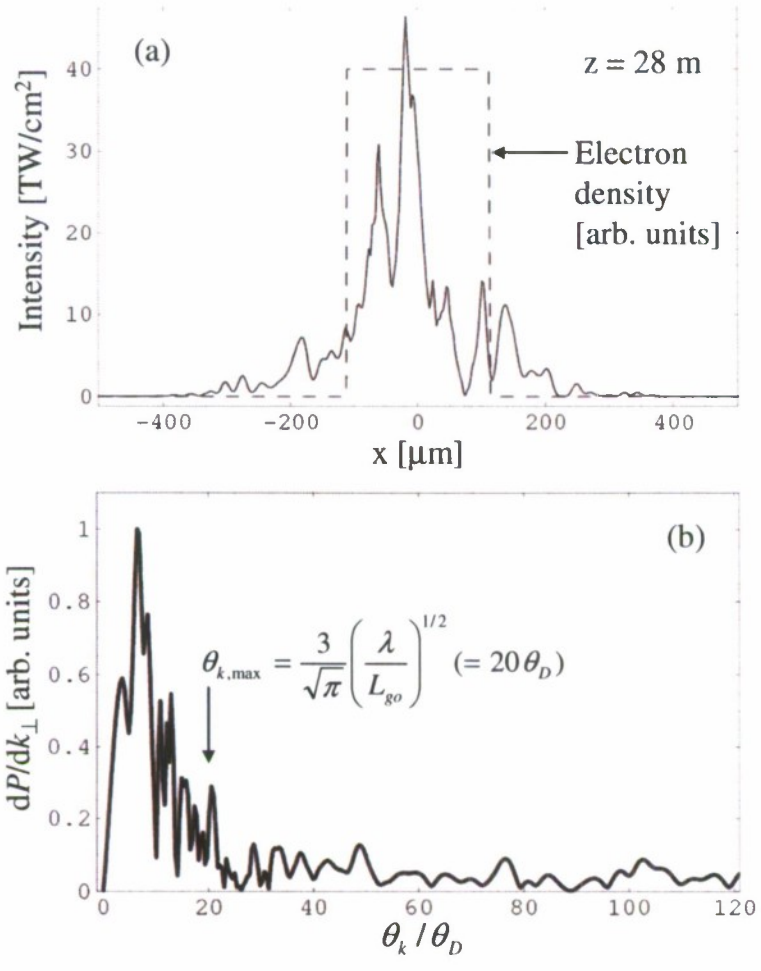

Figure 7: (a) GENESIS simulation result showing transverse profile of intensity (solid curve) at $z = 28$ m (saturation) for the LCLS FEL. Dashed curve denotes electron beam profile. (b) Distribution of power over normalized transverse wavenumber (propagation angle), for the intensity profile shown in (a). Propagation angle is normalized to the diffraction angle θ_D. $\theta_{k,\max}$ denotes the maximum propagation gain angle from Eq. (16).

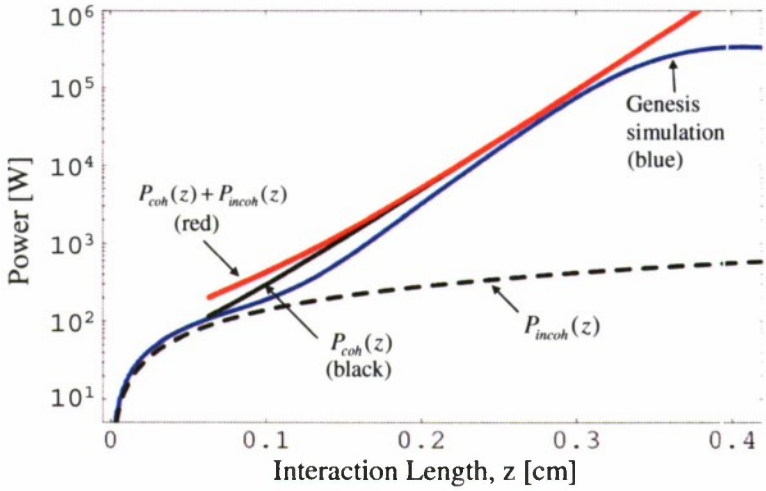

Figure 8: Power versus interaction length for a laser-pumped FEL (cold beam) with parameters listed in Table I. Curves denote coherent power (solid black), incoherent power (dashed), total theoretical power (red), and the result of a Genesis simulation (blue). The theoretical efficiency is $\eta = 0.023(\lambda_o / L_{go}) = 0.007\%$. The efficiency observed in the GENESIS simulation is 0.01%. In calculating the incoherent and coherent power from Eqs. (26) and (30), we used the maximum angle resolved by the simulation, i.e., $\theta_{sim} \approx \lambda/(2\Delta_x) = 5\times10^{-4}$ rad where $\Delta_x = 1.6$ μm is the transverse grid size. In this parameter regime, $\theta_{sim} << \theta_{k,\max}$, where $\theta_{k,\max}$ is the maximum propagation angle of the coherent radiation given by Eq. (16).

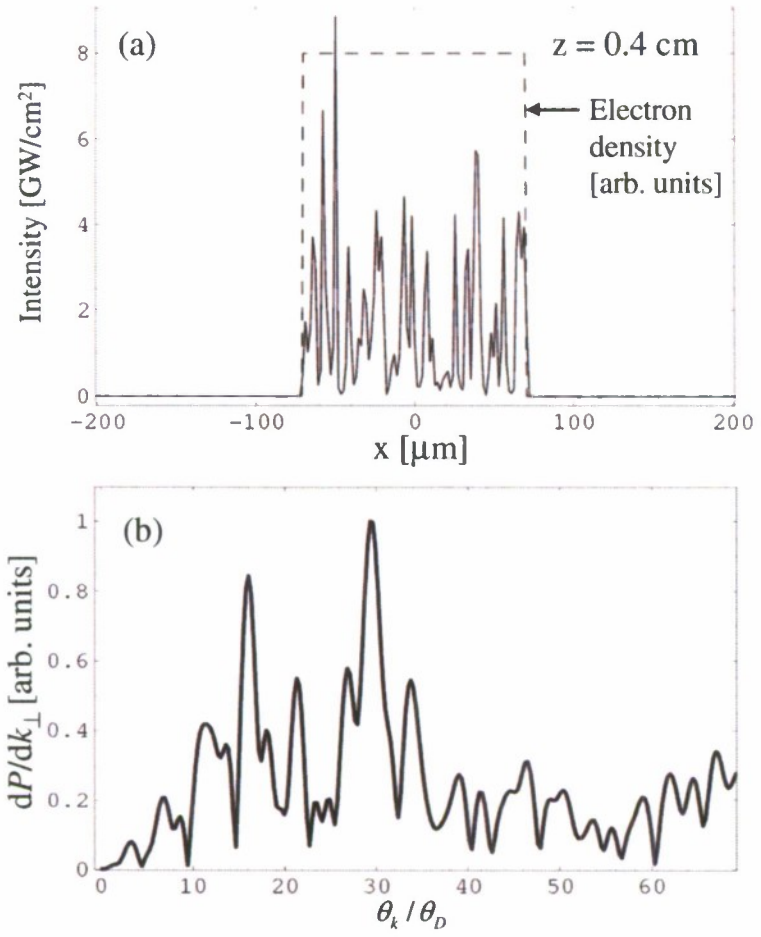

Figure 9: (a) GENESIS simulation result showing transverse profile of intensity (solid curve) at $z = 0.4$ cm (saturation) for the laser-pumped FEL. Dashed curve denotes electron beam profile. (b) Distribution of power over normalized transverse wavenumber (propagation angle), for the intensity profile shown in (a). Propagation angle is normalized to the diffraction angle θ_D. Maximum angle resolved by the simulation is $\theta_{k,\max} = 70\theta_D$. Maximum theoretical propagation angle is $\theta_{k,\max} \approx 500\theta_D$.